Available online at www.sciencedirect.com

ScienceDirect

International Journal of Solids and Structures 45 (2008) 2379–2398

INTERNATIONAL JOURNAL OF SOLIDS AND STRUCTURES

www.elsevier.com/locate/ijsolstr

A semi-analytic meshfree method for Almansi–Michell problems of piezoelectric cylinders

C.W. Liu, E. Taciroglu *

Department of Civil & Environmental Engineering, University of California, Los Angeles, CA 90095, USA

Received 11 September 2006; received in revised form 28 October 2007
Available online 14 December 2007

Abstract

Saint-Venant's Problem, Almansi–Michell Problems, Meshfree Methods, Piezoelectricity. We present a semi-analytical method for analyzing prismatic nonhomogeneous piezoelectric cylinders with arbitrary cross-sectional geometry. The prescribed loads considered in this study include axial forces, torques, moments, and voltage resultants prescribed at the cylinder's ends, as well as body forces, lateral surface shears, voltages, and pressures as long as they can be represented by a power series in the axial coordinate. This problem can be considered as an extension of Saint-Venant and Almansi–Michell problems for elastic bodies to piezoelectric bodies. In this computationally efficient method, the cross-sectional plane is discretized with a meshfree approach, and the solution is obtained analytically with respect to the axial coordinate. A number of examples are provided to demonstrate the veracity and utility of the proposed method.

Keywords: Piezoelectricity; Semi-analytic methods; Smart structures; Sensors; Actuators; Saint-Venant's problem; Almansi–Michell problems; Meshfree methods

1. Introduction

Piezoelectric materials are being utilized in a broad variety of active material systems due to the precision they afford, and their simultaneous sensing and actuation capabilities. Recent developments in this area indicate that significant gains in sensing and actuation capacities can be achieved with distributed and continuous (as opposed to discrete) placement of active materials within the host structure (see, for example, Cesnik and Shin, 2001). A significant portion of such 'smart' structures with integrated active materials possess prismatic (beam/plate-like) geometries; yet, by default, they have nonhomogeneous and highly anisotropic cross-sections.

The methods of analysis for the aforementioned type of smart structures can be classified into (I) analytical methods, which yield exact (or classical) solutions, (II) methods based on structural theories, (III) fully discrete (e.g., three-dimensional finite element) methods, and (IV) semi-analytical methods. These approaches

* Corresponding author. Tel.: +1 310 267 4655; fax: +1 310 206 2222.
E-mail address: etacir@ucla.edu (E. Taciroglu).

0020-7683/$ - see front matter
doi:10.1016/j.ijsolstr.2007.12.001

vary in attributes such as computational efficiency and accuracy. Classical solutions are the most accurate, and yet scarce, for obvious reasons. Fully discrete solutions are almost always possible to obtain, but also invariably are the most expensive. It is therefore natural that, in the area of smart structures and materials, the most popular methods belong to category II. This is mainly due to the efficiency these methods provide without sacrificing too much in accuracy. However, their range of applicability is limited by the constraining (e.g., kinematic) hypotheses with which they are generated. The method proposed in this study belong the last and the least explored category (IV), and it strikes a favorable balance between computational efficiency and accuracy. In what follows, we hope to illuminate the case in point by providing an overview of the said categories of methods. This overview is not meant to be comprehensive and is included to bring the present effort into perspective.

1.1. Classical solutions: a discussion of Saint-Venant's problem and its derivatives in relation to smart structures

Saint-Venant's problem (1855, 1856) is one of the most celebrated problems of three-dimensional elasticity. It is a boundary value problem involving a prismatic body (henceforth referred to as a cylinder) subject to surface tractions over its ends and with no body forces. As per this layout, many of the actuator/sensor devices with beam/plate geometries can be considered within the Saint-Venant paradigm.

The so-called 'relaxed formulation' of Saint-Venant's problem is the version where stress resultants (i.e., bending moments, torque, normal, and shear forces) rather than pointwise tractions are prescribed at the ends of the cylinder. On the other hand, the 'extended' Saint-Venant's problem, or the Almansi–Michell problem, deals with body forces and lateral tractions in addition to the end tractions. The particular naming is due to Almansi (1901) who considered lateral surface tractions that are linearly varying in the axial coordinate of the cylinder, and to Michell (1901) who treated uniform surface tractions only. Classical solutions to the relaxed formulation have been obtained through the 'semi-inverse' and 'generalized plane-strain' approaches in the past. The latter is the more powerful of the two, and is primarily due to Ieşan (1986, 1987). Pertinent to the proposed study, Ieşan's approach can be systematically extended to obtain solutions for arbitrary lateral surface tractions; and it can be used to formulate a semi-analytical method to handle nonhomogeneous cross-sections comprising materials with the most general form of anisotropy (see, for example, Dong et al., 2001). As might be expected of both of the said approaches in their purely analytical form, classical solutions are typically restricted to simple geometry and loading conditions such as circular tubes (Tarn, 2002), monoclinic crystals (Daví, 1996; Bisegna, 1998), etc. These solutions are extremely valuable however, as they constitute useful benchmarks for validating finite element and various beam and plate theory-based solutions.

1.2. Finite element methods and structural theories applied to smart structures

Perhaps the earliest work on continuum finite elements incorporating coupled electromechanical response is by Allik and Hughes (1970). Since then, numerous innovations taking place in finite element methods have been put to use in research on smart structures (for a recent survey see Benjeddou, 2000). Due to the high cost of three-dimensional numerical methods and the scarcity of classical solutions, beam, plate, and shell theories – referred herein as structural theories – are arguably the most commonly used tools for analysis, design and control of smart structures at present (see, for example, Saravanos and Heyliger, 1995; or see Saravanos and Heyliger, 1999; for a survey). A beam, plate or shell problem may be viewed as a constrained three-dimensional elasticity problem whereby the solutions are restricted usually by a hypothesis on deformations and by the simplification of boundary conditions as in the case of the relaxed Saint-Venant problem (Popescu and Hodges, 1999). Like any other constrained problem, determination of the range of validity of solutions based on structural theories is very important, as any subsequent analysis and design that falls outside this range is dubious.

1.3. Semi-analytic methods applied to smart structures and the present effort

The final, and presently the least explored, category is that of the semi-analytical methods for analysis of smart structures and heterogeneous material systems. We reserve the term 'semi-analytic' for methods in which the total solution is obtained by the simultaneous and consistent use of a numerical (e.g., finite element, mesh-

free, etc.) and an analytical method. Ideally, this is achieved in a modular fashion such that an analytical solution is obtained entirely in one or more dimensions thereby allowing that part of the solution to be built (or condensed) into the overall solution procedure. It should be noted that the ordinary plane-strain and axisymmetric finite element analyses belong to this category, as part of the solution is analytic in each case – albeit trivially via symmetry arguments. The advantages of semi-analytic methods are mainly twofold: (i) computational effort is reduced by one or more orders of magnitude; (ii) part of the behavior is obtained analytically and thus it is inherently more accurate than any numerical approximation. These advantages are attractive for smart structures – especially those with distributed sensor/actuator systems – enabling computation-intensive investigations such as design sensitivity analyses, topology optimization, or development of active control algorithms. Furthermore, semi-analytic solutions can be used to investigate the range of validity of *ad hoc* structural theories for heterogeneous material systems, and as a basis for the development of new ones.

The basis of the present work is due to Huang and Dong (2001) and Dong et al. (2001) who proposed a semi-analytical finite element method for obtaining the mechanical behavior of anisotropic cylinders due to end loads (i.e., Saint-Venant solutions). This approach was extended to the analysis of laminated *piezoelectric circular* cylinders subject to electromechanical end loadings by Taciroglu et al. (2004), Taciroglu and Liu (2005), and Liu and Taciroglu (2007). Building on this earlier work, herein we develop a semi-analytical method to obtain solutions for nonhomogeneous prismatic piezoelectric cylinders with *arbitrary cross-sectional geometry* under mechanical and electrical loads applied at the cylinder's ends and/or its lateral surfaces. The problem investigated here involves complex deformations due to bending and flexure which are absent in previous work; and determining the exact form of the displacement and electric potential fields for the anisotropic, nonhomogeneous beam is a non-trivial task. This problem can be considered as extensions of the Saint-Venant (1855, 1856) and, the more general, Almansi–Michell (1901) problems for elastic bodies to piezoelectric bodies. The solution methodology calls for the displacement and electric potential fields to be set forth at the outset. Ieşan's (1986) rational scheme is used to generate the functional forms of these fields, which has the advantage of being systematic (i.e., displacement and electric potential fields for higher-order problems can be generated from those of lower-order ones sequentially) and free of any *a priori* assumptions, such as those used in semi-inverse methods. For each of these sequential problems, the displacement and electric potential fields can be decomposed into primal, and cross-sectional fields. The primal field can be obtained from the kinematic hypotheses of elementary bar and beam theories. The cross-sectional field is independent of the axial coordinate and is determined by substituting the displacement and electric potential fields into the variational form of governing equations, which are discretized only in the cross-sectional plane using a meshfree method.

Work related to this type of theory has also been proposed by Yu et al. (2002) and Yu and Hodges (2004), who decompose the three-dimensional elasticity problem into a 2-D cross-sectional analysis, and a 1-D beam problem via the so-called "variational asymptotic method." Another group of researchers (Giavotto et al., 1983; Borri and Merlini, 1986; Ghiringhelli et al., 1997) presented a similar semi-analytical approach comprising, yet again, two main stages, which are the determination of the cross-sectional properties, and the evaluation of the structural response based on the computed properties. In this approach, the 6×6 cross-sectional flexibility matrix is computed by solving six canonical problems in Giavotto et al. (1983), or by introducing the concept of "intrinsic warping" in Borri and Merlini (1986). The Saint-Venant's solution is then obtained based on the calculated cross-sectional properties. This approach has also been extended to piezoelectric beams by Ghiringhelli et al. (1997). It is useful to point out the main differences between these works and our present approach. First, our approach is a method of undetermined coefficients whereby the solution vector satisfies the governing semi-analytical equations exactly (i.e., no *a priori* assumptions are made on stress distributions or cross-sectional deformations). Second, we can deal with lateral surface loads, while previous work only treats resultant end loads (i.e., Saint-Venant problems).

The proposed semi-analytical meshfree method is ideal for analysis and optimal design of prismatic structures containing distributed piezoelectric sensor/actuator devices because (i) the semi-analytical method allows a dimensional reduction without any loss of accuracy and thus, it provides significant savings in computation compared to three-dimensional numerical methods; and (ii) the sensitivities of externally defined design objective functions with respect to changes in structural topology or material attributes can be easily obtained through the meshfree approach (Bobaru and Mukherjee, 2001).

In what follows, we present the governing equations and general solution strategy in Sections 2 and 3. Rigid body modes, uniform and linear states are considered in Sections 4–6, respectively. A set of verification problems and an application example are provided in Section 7.

2. Governing equations

2.1. Problem statement

Consider a prismatic piezoelectric cylinder of length L with an arbitrary cross-sectional geometry as illustrated in Fig. 1a. The cylinder comprises an arbitrary number of materials – each of which may possess the most general form of anisotropy – and the material interfaces have arbitrary shapes. We adopt a Cartesian coordinate system (x, y, z) with its origin located at the centroid of the cross-section – a choice for which there is no restriction. The cylinder is mechanically restrained at the root-end ($z = L$), and free of mechanical displacement boundary conditions at the tip-end ($z = 0$). Extensions to other mechanical displacement boundary conditions, such as simple supports, and statically indeterminate problems can also be considered in the solution procedures that follow, and we shall omit the details of such cases for brevity.

The cylinder can be subjected to mechanical loads at its tip-end and on its lateral surface, and to electrical loads at its either end, its lateral surface, and throughout the material interfaces (via electrodes). Herein, we only consider the *resultants* of the electromechanical loads applied at the ends of the cylinder (i.e., the relaxed formulation of Saint-Venant's problem), and only such electromechanical loads – applied along the lateral surface of the cylinder – that have a polynomial variation in their magnitude along the z-axis (i.e., *extensions* of Almansi–Michell problems).

The linear constitutive equations of a piezoelectric material are given by

$$\mathbf{T} = \mathbf{C}^E\mathbf{S} - \mathbf{e}\mathbf{E}, \quad \mathbf{D} = \mathbf{e}^T\mathbf{S} + \boldsymbol{\kappa}^S\mathbf{E} \tag{1}$$

where the vectors denote the stresses $\mathbf{T} = [T_{xx}, T_{yy}, T_{zz}, T_{yz}, T_{xz}, T_{xy}]^{\mathrm{T}}$, electric displacements $\mathbf{D} = [D_x, D_y, D_z]^{\mathrm{T}}$, strains $\mathbf{S} = [S_{xx}, S_{yy}, S_{zz}, S_{yz}, S_{xz}, S_{xy}]^{\mathrm{T}}$, and electric field variables $\mathbf{E} = [E_x, E_y, E_z]^{\mathrm{T}}$; while the matrices $\mathbf{C}^E$, $\boldsymbol{\kappa}^S$, and $\mathbf{e}$ denote the elastic stiffness values measured at constant electric field, the dielectric permittivities at constant strain, and the electromechanical (piezoelectric) coupling constants, respectively. We choose the primary field variables as the mechanical displacements $\mathbf{u} = [u, v, w]^{\mathrm{T}}$ and the electric potential (voltage) ϕ. As such, it is convenient to group the dependent and independent variables as

$$\mathbf{q} = \begin{bmatrix} \mathbf{S} \\ \mathbf{E} \end{bmatrix}_{9\times 1}, \qquad \mathbf{Q} = \begin{bmatrix} \mathbf{T} \\ \mathbf{D} \end{bmatrix}_{9\times 1}, \qquad \mathbf{v} = \begin{bmatrix} \mathbf{u} \\ \phi \end{bmatrix}_{4\times 1}. \tag{2}$$

Then, the constitutive relationships in Eq. (1) may be restated compactly as

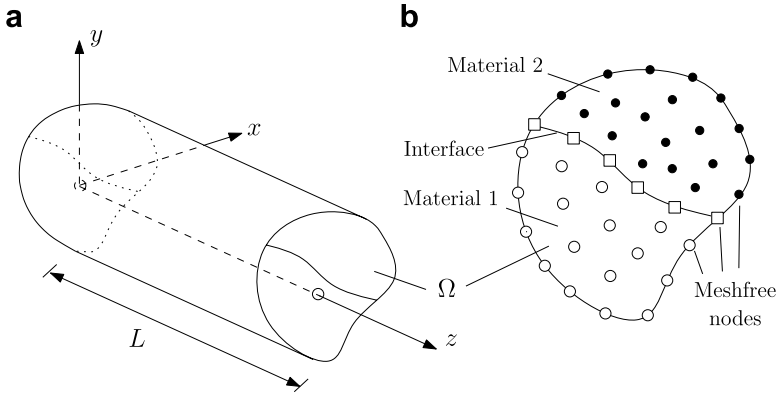

Fig. 1. Problem geometry and the coordinate system.

$$\mathbf{Q} = \mathbf{C}^{*}\mathbf{q} \quad \text{where} \quad \mathbf{C}^{*} = \begin{bmatrix} \mathbf{C}^{E} & -\mathbf{e} \\ \mathbf{e}^{T} & \boldsymbol{\kappa}^{S} \end{bmatrix}. \tag{3}$$

Moreover, the strain–displacement and electric field–potential relationships are given by

$$\mathbf{q} = \mathcal{L}\{\mathbf{v}\} = \left[\frac{1}{2}\left(\nabla\mathbf{u} + \nabla^{\mathrm{T}}\mathbf{u}\right), \quad -\nabla\phi\right]^{\mathrm{T}}. \tag{4}$$

2.2. Enriched reproducing kernel particle method

For the present study, we shall adopt a meshfree method to model the cross-sectional behavior. Meshfree methods – such as Element-Free Galerkin (Belytschko et al., 1994) and Reproducing Kernel Particle Methods (Liu et al., 1995) – have gained mainstream recognition within the last decade, and have been applied to numerous problems in continuum mechanics. These methods are ideal for adaptive computations and optimum design problems as because, in either of the aforementioned cases, nodes of the discrete model must be relocated, added or eliminated. With meshfree methods, these operations can be performed with ease in contrast to, for example, finite element methods which require remeshing.

Since basic meshfree methods employ smooth shape functions with overlapping supports, discontinuities in solution fields across material interfaces can not be interpolated properly. Several approaches have recently been developed to overcome this difficulty for purely mechanical problems (see, for example, Krongauz and Belytschko, 1998; Wang et al., 2003). Liu and Taciroglu (2006) have extended these approaches to electromechanical (plane-strain, plane-stress) problems involving arbitrarily shaped material interfaces, and proposed an enriched Reproducing Kernel Particle Method (eRKPM). In this study, we shall adopt this latter method to model the cross-sectional behavior. For the convenience of the reader, we provide the interpolation scheme (involving regular and enrichment functions) used in eRKPM here, and further details (such as interface curve representation, construction of enrichment functions, quadrature, assembly, etc.) may be found in Liu and Taciroglu (2006). For brevity, we present this interpolation scheme for a nonhomogeneous problem involving only two materials. The generalization of eRKPM to configurations with a larger number of distinct materials is straightforward; and should be apparent to the reader from the following discourse.

Consider a nonhomogeneous cylinder possessing two distinct piezoelectric materials within its cross-section as illustrated in Fig. 1b. The discretization consists two sets of particles: $S_{\mathrm{p}} = \{\mathbf{x}_1, \mathbf{x}_2, \cdots, \mathbf{x}_L\}$ (circles and dots in the figure), and $S_{\mathrm{c}} = \{\mathbf{x}_{L+1}, \mathbf{x}_{L+2}, \cdots, \mathbf{x}_{L+M}\}$ (squares in the figure), which are the particles within the piezoelectric/elastic domains, and those on the material interface, respectively. Identical shape functions are used to approximate the displacements and the electric potential as follows

$$u_i(x,y,z) = \sum_{I=1}^{L} \Psi_I(x,y)\tilde{d}_{iI}(z) + \sum_{I=L+1}^{L+M} \hat{\Psi}_I(x,y)\hat{d}_{iI}(z) \triangleq \sum_{I=1}^{N} \Phi_I(x,y)d_{iI}(z) \tag{5}$$

where $i \in \{1,2,3,4\}$. Here u_1, u_2, and u_3 are the three approximated displacement components; u_4 is the approximated electric potential field; Ψ_I, $\hat{\Psi}_I$, and Φ_I are the conventional RKPM shape functions, the interface enrichment functions (used for capturing discontinuities across the interface), and the overall (composite) enriched RKPM shape functions, respectively; $\tilde{d}_{iI}$, $\hat{d}_{iI}$, and d_{iI} are the associated nodal *coefficients* of these shape functions; and, $N = L + M$ is the total number of discretized particles. Further details of this interpolation scheme may be found in Liu and Taciroglu (2006).

2.3. Governing equations stated in a semi-analytical form

In the present study, we shall seek the solution in a semi-analytical form. To wit, we shall obtain the solution field using a combination of eRKPM in the cross-sectional coordinates, and an analytical method along the axial coordinate. To facilitate this approach, we decompose the linear differential operator $\mathcal{L}$ in Eq. (4) into two parts as in

$$\mathcal{L}\{\mathbf{v}\} = [\mathcal{L}_{xy} + \mathcal{L}_z]\{\mathbf{v}\} \tag{6}$$

where $\mathcal{L}_{xy}$ and $\mathcal{L}_z$ are given by (where a symbol '·' simply denotes a zero term)

$$\mathcal{L}_{xy} = \begin{bmatrix} \frac{\partial}{\partial x} & \cdot & \cdot & \cdot \\ \cdot & \frac{\partial}{\partial y} & \cdot & \cdot \\ \cdot & \cdot & \cdot & \cdot \\ \cdot & \cdot & \frac{\partial}{\partial y} & \cdot \\ \cdot & \cdot & \frac{\partial}{\partial x} & \cdot \\ \frac{\partial}{\partial y} & \frac{\partial}{\partial x} & \cdot & \cdot \\ \cdot & \cdot & \cdot & -\frac{\partial}{\partial x} \\ \cdot & \cdot & \cdot & -\frac{\partial}{\partial y} \\ \cdot & \cdot & \cdot & \cdot \end{bmatrix}, \qquad \mathcal{L}_z = \begin{bmatrix} \cdot & \cdot & \cdot & \cdot \\ \cdot & \cdot & \cdot & \cdot \\ \cdot & \cdot & \frac{\partial}{\partial z} & \cdot \\ \cdot & \frac{\partial}{\partial z} & \cdot & \cdot \\ \frac{\partial}{\partial z} & \cdot & \cdot & \cdot \\ \cdot & \cdot & \cdot & \cdot \\ \cdot & \cdot & \cdot & \cdot \\ \cdot & \cdot & \cdot & \cdot \\ \cdot & \cdot & \cdot & -\frac{\partial}{\partial z} \end{bmatrix}. \tag{7}$$

Substitution of Eq. (5) into Eq. (6) gives

$$\mathbf{q} = \sum_{I=1}^{N} \mathbf{B}_1^I \mathbf{d}_I + \sum_{I=1}^{N} \mathbf{B}_2^I \mathbf{d}_{I,z} \tag{8}$$

where

$$\mathbf{B}_1^I = \begin{bmatrix} \Phi_{I,x} & \cdot & \cdot & \cdot \\ \cdot & \Phi_{I,y} & \cdot & \cdot \\ \cdot & \cdot & \cdot & \cdot \\ \cdot & \cdot & \Phi_{I,y} & \cdot \\ \cdot & \cdot & \Phi_{I,x} & \cdot \\ \Phi_{I,y} & \Phi_{I,x} & \cdot & \cdot \\ \cdot & \cdot & \cdot & -\Phi_{I,x} \\ \cdot & \cdot & \cdot & -\Phi_{I,y} \\ \cdot & \cdot & \cdot & \cdot \end{bmatrix}, \qquad \mathbf{B}_2^I = \begin{bmatrix} \cdot & \cdot & \cdot & \cdot \\ \cdot & \cdot & \cdot & \cdot \\ \cdot & \cdot & \Phi_I & \cdot \\ \cdot & \Phi_I & \cdot & \cdot \\ \Phi_I & \cdot & \cdot & \cdot \\ \cdot & \cdot & \cdot & \cdot \\ \cdot & \cdot & \cdot & \cdot \\ \cdot & \cdot & \cdot & \cdot \\ \cdot & \cdot & \cdot & -\Phi_I \end{bmatrix}. \tag{9}$$

The governing equilibrium equations may be variationally derived from the theorem of minimum potential energy, as in

$$\delta\{H + W\} = \mathbf{0} \tag{10}$$

where H is the electric enthalpy (see, for example, Tiersten, 1969) given by

$$H = \int_0^L \int_\Omega \left(\frac{1}{2} \mathbf{q}^{\mathrm{T}} \mathbf{C}^* \mathbf{q} - \mathbf{E}^{\mathrm{T}} \mathbf{D} \right) \mathrm{d}\Omega \, \mathrm{d}z, \tag{11}$$

and W is the potential energy of mechanical and electrical loads. By inserting the expression of $\mathbf{q}$ in Eq. (8) into Eq. (11), and by carrying out the variation, we obtain the governing equilibrium equations in semi-analytic form as

$$\hat{\mathbf{K}}_1 \hat{\mathbf{V}}(z) + \hat{\mathbf{K}}_2 \hat{\mathbf{V}}(z)_{,z} - \hat{\mathbf{K}}_3 \hat{\mathbf{V}}(z)_{,zz} = \hat{\mathbf{F}}(z) \tag{12}$$

where $\hat{\mathbf{V}}$ is the assembled array of nodal coefficients associated with displacements and electric potentials, and $\hat{\mathbf{K}}_1$, $\hat{\mathbf{K}}_2$, and $\hat{\mathbf{K}}_3$ are system matrices given by

$$\hat{\mathbf{K}}_1^{IJ} = \int_\Omega \mathbf{B}_1^{I\,\mathrm{T}} \hat{\mathbf{C}} \mathbf{B}_1^J \,\mathrm{d}\Omega, \quad \hat{\mathbf{K}}_2^{IJ} = \int_\Omega \left[\mathbf{B}_1^{I\,\mathrm{T}} \hat{\mathbf{C}} \mathbf{B}_2^J - \mathbf{B}_2^{I\,\mathrm{T}} \hat{\mathbf{C}} \mathbf{B}_1^J\right] \mathrm{d}\Omega,$$
$$\hat{\mathbf{K}}_3^{IJ} = \int_\Omega \mathbf{B}_2^{I\,\mathrm{T}} \hat{\mathbf{C}} \mathbf{B}_2^J \,\mathrm{d}\Omega, \quad \hat{\mathbf{C}} = \begin{bmatrix} \mathbf{C}^E & -\mathbf{e} \\ -\mathbf{e}^T & -\boldsymbol{\kappa}^S \end{bmatrix}. \tag{13}$$

The relationships between the nodal values and nodal coefficients can be obtained through Eq. (5), i.e.,

$$u_i(x_J, y_J, z) = \sum_{I=1}^{N} \Phi_I(x_J, y_J) d_{iI}(z) \quad \Rightarrow \quad \hat{\mathbf{V}}(z) = \boldsymbol{\Lambda}^{-\mathrm{T}} \mathbf{V}(z) \tag{14}$$

where $\mathbf{V}$ is the assembled array of nodal displacements and electric potential; and $\boldsymbol{\Lambda}$ is the transformation matrix given by $\boldsymbol{\Lambda}_{IJ} = \Phi_I(x_J, y_J)\mathbf{I}$. Through a coordinate transformation, Eq. (12) can be restated as

$$\mathbf{K}_1 \mathbf{V}(z) + \mathbf{K}_2 \mathbf{V}(z)_{,z} - \mathbf{K}_3 \mathbf{V}(z)_{,zz} = \mathbf{F}(z) \tag{15}$$

where the electromechanical 'stiffness' matrices and 'force' vector are given by

$$\mathbf{K}_i = \boldsymbol{\Lambda}^{-1} \hat{\mathbf{K}}_i \boldsymbol{\Lambda}^{-\mathrm{T}} \quad i \in \{1,2,3\}, \quad \mathbf{F} = \boldsymbol{\Lambda}^{-1} \hat{\mathbf{F}}. \tag{16}$$

3. General solution strategy

We shall use a method of undetermined coefficients for solving the system of ordinary differential equations in Eq. (15). The analytical form of the solution field will be obtained via Ieşan's (1986) hierarchical approach. As such, the electromechanical load vector $\mathbf{F}(z)$ needs to be expressed as polynomials of z, that is

$$\mathbf{F}(z) = (\mathbf{F}_{0ma} + \mathbf{F}_{0e}) + (\mathbf{F}_{0mb} + z\mathbf{F}_{1ma} + z\mathbf{F}_{1e}) + \cdots + (z^{k-1}\mathbf{F}_{(k-1)mb} + z^k \mathbf{F}_{kma} + z^k \mathbf{F}_{ke})$$
$$k \in \{0,1,2,\cdots\}. \tag{17}$$

Here, the subscripts m and e denote the mechanical and electric loads, respectively; $\mathbf{F}_{kma}$ denotes the loads that are devoid of any resultant force or moment in the z-direction, such as uniform pressure ($k = 0$), linear pressure ($k = 1$), etc.; $\mathbf{F}_{kmb}$ denotes the loads that have such resultants, such as axial surface shear tractions; and finally $\mathbf{F}_{ke}$ denotes the electric loads, such as uniform voltage ($k = 0$), linear voltage ($k = 1$) applied along the z-direction. Correspondingly, the solution field to Eq. (15) due to loads given in the form of Eq. (17) can be stated as

$$\mathbf{V}(z) = \mathbf{V}_0(z) + \mathbf{V}_1(z) + \cdots + \mathbf{V}_k(z) + \cdots \tag{18}$$

where each component $\mathbf{V}_k(z)$ represents a particular axial variation of the solution fields; i.e., $\mathbf{V}_0(z)$ represents a uniform state, $\mathbf{V}_1(z)$ a linear state, and so forth. Here, we use the term "uniform state" to mean a *uniform stress and electric displacement state* for brevity (and the same terminology applies to linear state, quadratic state, and so forth).

Upon substituting Eqs. (17) and (18) into Eq. (15), we may decompose the governing equations as

$$\begin{aligned}
&\mathbf{K_1}\mathbf{V}_0 + \mathbf{K_2}\mathbf{V}_{0,z} - \mathbf{K_3}\mathbf{V}_{0,zz} = \mathbf{F}_{0ma} + \mathbf{F}_{0e}, \quad (0) \\
&\mathbf{K_1}\mathbf{V}_1 + \mathbf{K_2}\mathbf{V}_{1,z} - \mathbf{K_3}\mathbf{V}_{1,zz} = \mathbf{F}_{0mb} + z\mathbf{F}_{1ma} + z\mathbf{F}_{1e}, \quad (1) \\
&\qquad\qquad\qquad\qquad\qquad\qquad \vdots \\
&\mathbf{K_1}\mathbf{V}_k + \mathbf{K_2}\mathbf{V}_{k,z} - \mathbf{K_3}\mathbf{V}_{k,zz} = z^{k-1}\mathbf{F}_{(k-1)mb} + z^k\mathbf{F}_{kma} + z^k\mathbf{F}_{ke}. \quad (k)
\end{aligned} \tag{19}$$

The solution of these equations can be obtained by sequentially solving for $\mathbf{V}_0$, $\mathbf{V}_1$, and so on, up to the k-th order depending on the loads. Prescribed end conditions must be well-defined and global equilibrium must be satisfied for every equation in Eq. (19). As mentioned perviously, we shall seek a relaxed solution whereby the resultants of electric displacement and tractions, rather than their pointwise values, at the cylinder's ends are accounted for. These resultants over a cross-section at any station z along the length of this cylinder are given by the integrals

$$
\begin{aligned}
P_x(z) &= \int_\Omega T_{xz}(z)\,\mathrm{d}x\,\mathrm{d}y, \quad \overline{D}_x(z) = \int_\Omega D_x(z)\,\mathrm{d}x\,\mathrm{d}y,\\
P_y(z) &= \int_\Omega T_{yz}(z)\,\mathrm{d}x\,\mathrm{d}y, \quad \overline{D}_y(z) = \int_\Omega D_y(z)\,\mathrm{d}x\,\mathrm{d}y,\\
P_z(z) &= \int_\Omega T_{zz}(z)\,\mathrm{d}x\,\mathrm{d}y, \quad \overline{D}_z(z) = \int_\Omega D_z(z)\,\mathrm{d}x\,\mathrm{d}y,\\
M_x(z) &= \int_\Omega T_{zz}(z) y\,\mathrm{d}x\,\mathrm{d}y, \quad M_y(z) = -\int_\Omega T_{zz}(z) x\,\mathrm{d}x\,\mathrm{d}y,\\
M_z(z) &= \int_\Omega (T_{yz}(z)x - T_{xz}(z)y)\,\mathrm{d}x\,\mathrm{d}y.
\end{aligned}
\tag{20}
$$

In Sections 4–6, we present solutions to the first two stages (i.e., $k = 0$, and $k = 1$) of Eq. (19) to demonstrate the proposed method. Determination of the solutions for $k \geqslant 2$ should be apparent from this discourse.

4. Rigid body motions

Following Ieşan (1986), the form of the solution vector $\mathbf{V}_k$ for any given stage can be obtained by integrating the previous stage's solution vector once with respect to z (i.e., $\mathbf{V}_k = \int \mathbf{V}_{k-1}\,\mathrm{d}z$); and the form of the solution vector for the first stage ($\mathbf{V}_0$) is computed by integrating the rigid body modes ($\mathbf{V}_{-1} \equiv \mathbf{V}_{\mathrm{RB}}$) once with respect to z. It should be noted here that the aforementioned integrals are indefinite and merely yield the *functional form* of $\mathbf{V}_k$ with its unknown coefficients to be determined from the global equilibrium equations and the given boundary conditions.

For the present problem, there are seven rigid body modes (i.e., six stress-free kinematic modes, and one electric displacement-free voltage mode), and they may be formed (up to an arbitrary constant) as in

$$
\mathbf{V}_{\mathrm{RB}} = a_{01}\mathbf{R}_1 + a_{02}\mathbf{R}_2 + a_{03}\mathbf{R}_3 + a_{04}\mathbf{R}_4 + a_{05}\mathbf{R}_5 + a_{06}\mathbf{R}_6 + a_{07}\mathbf{R}_7 - (a_{04}\mathbf{R}_2 + a_{05}\mathbf{R}_1)z \tag{21}
$$

where a_{0i} ($i \in \{1,2,3\}$), a_{0j} ($j \in \{4,5,6\}$), and a_{07} are the translational, rotational, and electric potential (voltage) amplitudes, respectively. The vectors of rigid body modes are given by

$$
\begin{aligned}
&\mathbf{R}_1^{\mathrm{T}} = [\mathbf{I},\mathbf{0},\mathbf{0},\mathbf{0}], \mathbf{R}_2^{\mathrm{T}} = [\mathbf{0},\mathbf{I},\mathbf{0},\mathbf{0}], \mathbf{R}_3^{\mathrm{T}} = [\mathbf{0},\mathbf{0},\mathbf{I},\mathbf{0}], \mathbf{R}_7^{\mathrm{T}} = [\mathbf{0},\mathbf{0},\mathbf{0},\mathbf{I}],\\
&\mathbf{R}_4^{\mathrm{T}} = [\mathbf{0},\mathbf{0},\mathbf{y},\mathbf{0}], \mathbf{R}_5^{\mathrm{T}} = [\mathbf{0},\mathbf{0},\mathbf{x},\mathbf{0}], \mathbf{R}_6^{\mathrm{T}} = [-\mathbf{y},\mathbf{x},\mathbf{0},\mathbf{0}]
\end{aligned}
\tag{22}
$$

with row vectors $\mathbf{I}$, $\mathbf{x}$, and $\mathbf{y}$ containing N unit entries, the x and the it y-coordinates of the N meshfree particles, respectively. Here, we note that the 'rigid' electrical mode ($\mathbf{R}_7$) is given simply in the form of a constant potential throughout the whole cylinder; and it induces zero stresses and electric displacements. Substituting Eq. (21) into the homogeneous form of the governing Eq. (15) yields the following useful identities

$$
\mathbf{K}_1\mathbf{R}_i = \mathbf{0}\ (i \in \{1,2,3,6,7\}), \quad \mathbf{K}_1\mathbf{R}_4 = \mathbf{K}_2\mathbf{R}_2, \quad \mathbf{K}_1\mathbf{R}_5 = \mathbf{K}_2\mathbf{R}_1. \tag{23}
$$

5. Uniform state

The uniform state ($k = 0$) is governed by the first equation in Eq. (19), which is reproduced here by

$$
\mathbf{K_1}\mathbf{V}_0 + \mathbf{K_2}\mathbf{V}_{0,z} - \mathbf{K_3}\mathbf{V}_{0,zz} = \mathbf{F}_{0ma} + \mathbf{F}_{0e}. \tag{24}
$$

The mechanical load vector $\mathbf{F}_{0ma}$ represents a uniform pressure and exhibits no resultant axial force or torque. The electrical loads, $\mathbf{F}_{0e}$, may be decomposed into K load vectors as in

$$
\mathbf{F}_{0e} = \sum_{i=1}^{K} c_{1i}\mathbf{f}_{0ei} \tag{25}
$$

where K is the number of the meshfree particles where electrical loads are applied; and the vector $\mathbf{f}_{0ei}$ contains only a unit charge in the appropriate degree-of-freedom with the unknown coefficients c_{1i} to be determined

later. At this stage, axial force P_z, torque M_z, bending moments M_x and M_y, as well as voltage may be applied at the tip-end $z = 0$.

5.1. Analysis

The form of the most general solution vector to Eq. (24) can be obtained by integrating Eq. (21) once with respect to z

$$\mathbf{V}_0 = \sum_j a_{1j}(z\mathbf{R}_j + \mathbf{\Psi}_{1j}) + a_{14}\left(-\frac{z^2}{2}\mathbf{R}_2 + z\mathbf{R}_4 + \mathbf{\Psi}_{14}\right) + a_{15}\left(-\frac{z^2}{2}\mathbf{R}_1 + z\mathbf{R}_5 + \mathbf{\Psi}_{15}\right) + \mathbf{U}_{1m} + \sum_{i=1}^{K} c_{1i}\mathbf{\Psi}_{1ei} + \mathbf{V}_{\mathrm{RB}} \tag{26}$$

where $j \in \{1,2,3,6,7\}$. The generalized deformation coordinates a_{11} and a_{12} are associated with longitudinal shear, a_{13} with extension, a_{14} and a_{15} with bending, a_{16} with torsion, and a_{17} with primary potential field. $\mathbf{\Psi}_{1i}$ ($i \in \{1,\ldots,7\}$) and $\mathbf{U}_{1m}$ represent cross-sectional warpages and the particular solution for mechanical loads $\mathbf{F}_{0ma}$, respectively. The vectors $\mathbf{\Psi}_{1ei}$ along with amplitudes c_{1i} represent the response to electric loading $\mathbf{F}_{0e}$. Lastly, $\mathbf{V}_{RB}$ is a rigid body displacement whose coefficients, a_{0i} ($i \in \{1,\ldots,6\}$), depend on the restraint conditions at the root-end of the cylinder. Substituting Eq. (26) into Eq. (24) and applying the identities in Eq. (23) yield

$$\sum_j a_{1j}(\mathbf{K}_1\mathbf{\Psi}_{1j} + \mathbf{K}_2\mathbf{R}_j) + a_{14}(\mathbf{K}_1\mathbf{\Psi}_{14} + \mathbf{K}_2\mathbf{R}_4 + \mathbf{K}_3\mathbf{R}_2) + a_{15}(\mathbf{K}_1\mathbf{\Psi}_{15} + \mathbf{K}_2\mathbf{R}_5 + \mathbf{K}_3\mathbf{R}_1) + (\mathbf{K}_1\mathbf{U}_{1m} - \mathbf{F}_{0ma}) + \sum_{i=1}^{K} c_{1i}(\mathbf{K}_1\mathbf{\Psi}_{1ei} - \mathbf{f}_{0ei}) = \mathbf{0}, \quad j \in \{1,2,3,6,7\}. \tag{27}$$

In order to satisfy Eq. (27), the bracketed terms must vanish. The warpages $\mathbf{\Psi}_{1i}$, the particular solution $\mathbf{U}_{1m}$, and the electric response $\mathbf{\Psi}_{1ei}$ can then be determined by solving

$$\begin{aligned} &\mathbf{K}_1\mathbf{\Psi}_{1i} = -\mathbf{K}_2\mathbf{R}_i, \quad i \in \{1,2,3,6,7\},\\ &\mathbf{K}_1\mathbf{\Psi}_{14} = -\mathbf{K}_2\mathbf{R}_4 - \mathbf{K}_3\mathbf{R}_2, \quad \mathbf{K}_1\mathbf{\Psi}_{15} = -\mathbf{K}_2\mathbf{R}_5 - \mathbf{K}_3\mathbf{R}_1,\\ &\mathbf{K}_1\mathbf{U}_{1m} = \mathbf{F}_{0ma}, \quad \mathbf{K}_1\mathbf{\Psi}_{1ei} = \mathbf{f}_{0ei}, \quad i \in \{1,\ldots,K\}. \end{aligned} \tag{28}$$

Noting that $\mathbf{\Psi}_{11}$ and $\mathbf{\Psi}_{12}$ in Eq. (28) satisfy the last two rigid body identities in Eq. (23), we obtain

$$\mathbf{\Psi}_{11} = -\mathbf{R}_5, \quad \mathbf{\Psi}_{12} = -\mathbf{R}_4. \tag{29}$$

This result suggests that the first two terms in Eq. (26) can be classified as rigid body motions and added to the term $\mathbf{V}_{\mathrm{RB}}$. In other words, the two longitudinal shear fields, T_{xz} and T_{yz}, which are associated with a_{11} and a_{12}, vanish and are not involved in this ($k = 0$) problem.

After determining these distributions, the combined vector of nodal stresses and the electric displacements ($\mathbf{Q}$) can be constructed through Eq. (8)

$$\mathbf{Q} = \mathbf{C}^* \sum_{I=1}^{N} \left[\sum_{i=3}^{7} a_{1i}(\mathbf{B}_1^I\boldsymbol{\psi}_{1iI} + \mathbf{B}_2^I\mathbf{r}_{iI}) + \mathbf{B}_1^I\mathbf{u}_{1mI} + \sum_{i=1}^{K} c_{1i}\mathbf{B}_1^I\boldsymbol{\psi}_{1eiI} \right] \tag{30}$$

where, $\boldsymbol{\psi}_{1iI}$, $\mathbf{r}_{iI}$, $\mathbf{u}_{1mI}$, and $\boldsymbol{\psi}_{1eiI}$ are the I-th nodal components extracted from those distributions denoted by their corresponding upper case symbols, respectively. Here, we note that the following identities have been applied

$$\begin{aligned} &\sum_{I=1}^{N} \mathbf{B}_1^I\mathbf{r}_{iI} = \mathbf{0}, \quad i \in \{1,2,3,6,7\},\\ &\sum_{I=1}^{N} \mathbf{B}_1^I\mathbf{r}_{4I} = \sum_{I=1}^{N} \mathbf{B}_2^I\mathbf{r}_{2I}, \quad \sum_{I=1}^{N} \mathbf{B}_1^I\mathbf{r}_{5I} = \sum_{I=1}^{N} \mathbf{B}_2^I\mathbf{r}_{1I} \end{aligned} \tag{31}$$

in the construction of Eq. (30). Using the expression of $\mathbf{Q}$ and Eq. (20), the mechanical and the electric displacement resultants in the z-direction (the latter denoted by D), over any generic cross-section may be determined from

$$\mathbf{P} = \boldsymbol{\kappa}_I \mathbf{a}_I + \mathbf{P}_{Im} + \mathbf{P}_{Ie}\mathbf{c}_I \tag{32}$$

where the cross-sectional stiffness influence coefficients (κ_{Iij}) are given by

$$\begin{aligned}
\kappa_{I3j} &= \int_\Omega \mathbf{C}^*[\mathcal{L}_{xy}(\boldsymbol{\Psi}_{1j}) + \mathcal{L}_z(z\mathbf{R}_j)]_{(3)}\,\mathrm{d}x\,\mathrm{d}y,\\
\kappa_{I4j} &= \int_\Omega \mathbf{C}^*\left[\mathcal{L}_{xy}(\boldsymbol{\Psi}_{1j}) + \mathcal{L}_z(z\mathbf{R}_j)\right]_{(3)} y\,\mathrm{d}x\,\mathrm{d}y,\\
\kappa_{I5j} &= \int_\Omega \mathbf{C}^*[\mathcal{L}_{xy}(\boldsymbol{\Psi}_{1j}) + \mathcal{L}_z(z\mathbf{R}_j)]_{(3)} x\,\mathrm{d}x\,\mathrm{d}y,\\
\kappa_{I6j} &= \int_\Omega \mathbf{C}^*\{[\mathcal{L}_{xy}(\boldsymbol{\Psi}_{1j}) + \mathcal{L}_z(z\mathbf{R}_j)]_{(4)} x - [\mathcal{L}_{xy}(\boldsymbol{\Psi}_{1j}) + \mathcal{L}_z(z\mathbf{R}_j)]_{(5)} y\}\,\mathrm{d}x\,\mathrm{d}y,\\
\kappa_{I7j} &= \int_\Omega \mathbf{C}^*[\mathcal{L}_{xy}(\boldsymbol{\Psi}_{1j}) + \mathcal{L}_z(z\mathbf{R}_j)]_{(9)}\,\mathrm{d}x\,\mathrm{d}y,
\end{aligned} \tag{33}$$

with $i,j \in \{3,\ldots,7\}$. The unknown coefficient vectors $\mathbf{a}_I = [a_{13},\ldots,a_{17}]^{\mathrm{T}}$ and $\mathbf{c}_I = [c_{11},\ldots,c_{1K}]^{\mathrm{T}}$ have the dimensions of 5 and K, respectively. The resultants of the responses to the mechanical and electrical loads, $\mathbf{P}_{Im}$ and $\mathbf{P}_{Ie}$, are given by

$$\begin{aligned}
\mathbf{P}_{Im}(1) &= \int_\Omega \mathbf{C}^*[\mathcal{L}_{xy}(\mathbf{U}_{1m})]_{(3)}\,\mathrm{d}x\,\mathrm{d}y,\\
\mathbf{P}_{Im}(2) &= \int_\Omega \mathbf{C}^*[\mathcal{L}_{xy}(\mathbf{U}_{1m})]_{(3)} y\,\mathrm{d}x\,\mathrm{d}y,\\
\mathbf{P}_{Im}(3) &= \int_\Omega \mathbf{C}^*[\mathcal{L}_{xy}(\mathbf{U}_{1m})]_{(3)} x\,\mathrm{d}x\,\mathrm{d}y,\\
\mathbf{P}_{Im}(4) &= \int_\Omega \mathbf{C}^*\{[\mathcal{L}_{xy}(\mathbf{U}_{1m})]_{(4)} x - [\mathcal{L}_{xy}(\mathbf{U}_{1m})]_{(5)} y\}\,\mathrm{d}x\,\mathrm{d}y,\\
\mathbf{P}_{Im}(5) &= \int_\Omega \mathbf{C}^*[\mathcal{L}_{xy}(\mathbf{U}_{1m})]_{(9)}\,\mathrm{d}x\,\mathrm{d}y,
\end{aligned} \tag{34}$$

and

$$\begin{aligned}
\mathbf{P}_{Ie}(1,i) &= \int_\Omega \mathbf{C}^*[\mathcal{L}_{xy}(\boldsymbol{\Psi}_{1ei})]_{(3)}\,\mathrm{d}x\,\mathrm{d}y,\\
\mathbf{P}_{Ie}(2,i) &= \int_\Omega \mathbf{C}^*[\mathcal{L}_{xy}(\boldsymbol{\Psi}_{1ei})]_{(3)} y\,\mathrm{d}x\,\mathrm{d}y,\\
\mathbf{P}_{Ie}(3,i) &= \int_\Omega \mathbf{C}^*[\mathcal{L}_{xy}(\boldsymbol{\Psi}_{1ei})]_{(3)} x\,\mathrm{d}x\,\mathrm{d}y,\\
\mathbf{P}_{Ie}(4,i) &= \int_\Omega \mathbf{C}^*\{[\mathcal{L}_{xy}(\boldsymbol{\Psi}_{1ei})]_{(4)} x - [\mathcal{L}_{xy}(\boldsymbol{\Psi}_{1ei})]_{(5)} y\}\,\mathrm{d}x\,\mathrm{d}y,\\
\mathbf{P}_{Ie}(5,i) &= \int_\Omega \mathbf{C}^*[\mathcal{L}_{xy}(\boldsymbol{\Psi}_{1ei})]_{(9)}\,\mathrm{d}x\,\mathrm{d}y.
\end{aligned} \tag{35}$$

Here we note that the subscript (i) in Eqs. (33)–(35) indicates the i-th component of vector $\mathbf{q}$. All of the terms in Eq. (26) are known except the coefficients, which can be determined through the global equilibrium and the prescribed electrical conditions. We illustrate this procedure, in the absence and the presence of electric inputs respectively, in the following two subsections.

5.2. No electric inputs

In this case, the electric terms associated with c_{1i} ($i \in \{1,\ldots,K\}$) in Eq. (26) will vanish. Thus, the coefficients $\mathbf{a}_I$ in Eq. (32) can be obtained through the global equilibrium

$$\boldsymbol{\kappa}_I \mathbf{a}_I = \hat{\mathbf{P}}_I - \mathbf{P}_{Im} \tag{36}$$

where $\hat{\mathbf{P}}_I = [\hat{P}_z, \hat{M}_x, \hat{M}_y, \hat{M}_z, 0]^{\mathrm{T}}$ involve the applied axial end force and three end moments.

5.3. With electric inputs

Suppose that voltages are applied uniformly along the cylinder, which brings forth the K discretized conditions via Eq. (26) as

$$\hat{\phi}_k = a_{13}\psi_{13}(\mathbf{x}_k) + a_{14}\psi_{14}(\mathbf{x}_k) + a_{15}\psi_{15}(\mathbf{x}_k) + a_{16}\psi_{16}(\mathbf{x}_k) + \psi_{1m}(\mathbf{x}_k) + \sum_{i=1}^{K} c_{1i}\psi_{1ei}(\mathbf{x}_k), \quad k \in \{1,2,\ldots,K\} \tag{37}$$

where $\psi_{1i}(\mathbf{x}_k)$ ($i \in \{3,\ldots,6\}$), $\psi_{1m}(\mathbf{x}_k)$, and $\psi_{1ei}(\mathbf{x}_k)$ ($i \in \{1,\ldots,K\}$) are the potential values at point $\mathbf{x}_k$ extracted from the corresponding warpage vectors $\boldsymbol{\Psi}_{1i}$ ($i \in \{3,\ldots,6\}$), from the particular solution vector $\mathbf{U}_{1m}$ and from the electric response vectors $\boldsymbol{\Psi}_{1ei}$ ($i \in \{1,\ldots,K\}$), respectively; $\hat{\phi}_k$ is the applied voltage condition at k-th particle. Noting that, for the present case, the terms associated with c_{1i} ($i \in \{1,\ldots K\}$) in Eq. (26) account for the electric response, and thus, the term associated with a_{17} will vanish. Combining Eq. (37) with Eq. (32) yields $K+4$ equations for determining the $K+4$ coefficients, which are expressed here explicitly as

$$\begin{bmatrix} \boldsymbol{\kappa}_I(3:6,3:6) & \mathbf{P}_{Ie}(1:4,1:K) \\ \boldsymbol{\Psi}_I(3:6,1:K)^{\mathrm{T}} & \boldsymbol{\Psi}_{Ie}(1:K,1:K) \end{bmatrix} \begin{bmatrix} \mathbf{a}_I(1:4) \\ \mathbf{c}_I(1:K) \end{bmatrix} = \begin{bmatrix} \hat{\mathbf{P}}(1:4) - \mathbf{P}_{Im}(1:4) \\ \hat{\boldsymbol{\phi}}(1:K) - \boldsymbol{\psi}_{Im}(1:K) \end{bmatrix} \tag{38}$$

where

$$\boldsymbol{\Psi}_I(i,k) = \psi_{1i}(\mathbf{x}_k); \quad \boldsymbol{\Psi}_{Ie}(i,k) = \psi_{1ei}(\mathbf{x}_k); \quad \hat{\phi}(k) = \hat{\phi}_k; \quad \boldsymbol{\psi}_{Im}(k) = \psi_{1m}(\mathbf{x}_k). \tag{39}$$

6. Linear state

The linear state ($k=1$) is governed by the second equation in Eq. (19), which is reproduced here by

$$\mathbf{K_1}\mathbf{V}_1 + \mathbf{K_2}\mathbf{V}_{1,z} - \mathbf{K_3}\mathbf{V}_{1,zz} = \mathbf{F}_{0mb} + z\mathbf{F}_{1ma} + z\mathbf{F}_{1e} \tag{40}$$

where $\mathbf{F}_{1ma}$, $\mathbf{F}_{0mb}$, and $\mathbf{F}_{1e}$ are the linear pressure, uniform axial and torsional shears, and linear voltage load, respectively.

6.1. Analysis

The form of most general solution vector to Eq. (40) can be obtained by integrating Eq. (26) once with respect to z

$$\begin{aligned} \mathbf{V}_1 = {} & \sum_j a_{1j}\left(\frac{z^2}{2}\mathbf{R}_j + z\boldsymbol{\Psi}_{1j} + \boldsymbol{\Psi}_{2j}\right) + a_{14}\left(-\frac{z^3}{6}\mathbf{R}_2 + \frac{z^2}{2}\mathbf{R}_4 + z\boldsymbol{\Psi}_{14} + \boldsymbol{\Psi}_{24}\right) \\ & + a_{15}\left(-\frac{z^3}{6}\mathbf{R}_1 + \frac{z^2}{2}\mathbf{R}_5 + z\boldsymbol{\Psi}_{15} + \boldsymbol{\Psi}_{25}\right) + \sum_j a_{2j}\left(z\mathbf{R}_j + \boldsymbol{\Psi}_{1j}\right) \\ & + a_{24}\left(-\frac{z^2}{2}\mathbf{R}_2 + z\mathbf{R}_4 + \boldsymbol{\Psi}_{14}\right) + a_{25}\left(-\frac{z^2}{2}\mathbf{R}_1 + z\mathbf{R}_5 + \boldsymbol{\Psi}_{15}\right) \\ & + z\mathbf{U}_{2m1} + \mathbf{U}_{2m2} + \sum_{i=1}^{K} c_{1i}(z\boldsymbol{\Psi}_{1ei} + \boldsymbol{\Psi}_{2ei}) + \sum_{i=1}^{K} c_{2i}\boldsymbol{\Psi}_{1ei} + \mathbf{V}_{\mathrm{RB}} \end{aligned} \tag{41}$$

where $j \in \{1,2,3,6,7\}$. In this expression, a_{1i} and a_{2i} ($i \in \{1,\ldots,7\}$) as well as c_{1i} and c_{2i} ($i \in \{1,\ldots,K\}$) are the *new* generalized unknown coefficients (they are completely unrelated to the values of uniform state); $\mathbf{\Psi}_{2i}$ ($i \in \{1,\ldots,7\}$) and $\mathbf{\Psi}_{2ei}$ ($i \in \{1,\ldots,K\}$) are the *new* introduced warpages and electric responses, respectively; and, finally, $\mathbf{U}_{2m1}$ and $\mathbf{U}_{2m2}$ are particular solutions for the mechanical loads. All other vectors appearing in Eq. (41) are identical to their counterparts in the uniform-state problem. Substituting Eq. (41) into Eq. (40) yields the following equations, from which the new warpages, electric responses, and particular solutions can be determined,

$$\begin{aligned}
&\mathbf{K}_1\mathbf{\Psi}_{2i} = -\mathbf{K}_2\mathbf{\Psi}_{1i} + \mathbf{K}_3\mathbf{R}_i \quad i \in \{1,\ldots,7\},\\
&\mathbf{K}_1\mathbf{\Psi}_{2ei} = -\mathbf{K}_2\mathbf{\Psi}_{1ei} \quad i \in \{1,\ldots,K\},\\
&\mathbf{K}_1\mathbf{U}_{2m1} = \mathbf{F}_{1ma}, \quad \mathbf{K}_1\mathbf{U}_{2m2} + \mathbf{K}_2\mathbf{U}_{2m1} = \mathbf{F}_{0mb}.
\end{aligned} \tag{42}$$

Similarly, the vector of nodal stresses and electric displacements can be formed as

$$\begin{aligned}
\mathbf{Q} = \mathbf{C}^* \sum_{I=1}^{N} \{ & z\mathbf{B}_1^I\mathbf{u}_{2m1I} + \mathbf{B}_1^I\mathbf{u}_{2m2I} + \mathbf{B}_2^I\mathbf{u}_{2m1I}\\
&+ \sum_{i=3}^{7}[(za_{1i}+a_{2i})(\mathbf{B}_1^I\boldsymbol{\psi}_{1iI} + \mathbf{B}_2^I\mathbf{r}_{iI}) + a_{1i}(\mathbf{B}_1^I\boldsymbol{\psi}_{2iI} + \mathbf{B}_2^I\boldsymbol{\psi}_{1iI})]\\
&+ \sum_{i=1}^{K}[(zc_{1i}+c_{2i})\mathbf{B}_1^I\boldsymbol{\psi}_{1eiI} + c_{1i}(\mathbf{B}_1^I\boldsymbol{\psi}_{2eiI} + \mathbf{B}_2^I\boldsymbol{\psi}_{1eiI})]\}.
\end{aligned} \tag{43}$$

where we note that the terms related to a_{11}, a_{12}, a_{21}, and a_{22} have vanished in the expression of $\mathbf{Q}$. The linearly varying resultants can be obtained through Eq. (20), which yields

$$\mathbf{P} = z(\boldsymbol{\kappa}_I\mathbf{a}_I + \mathbf{P}_{IIm1}) + \boldsymbol{\kappa}_{II}\mathbf{a}_I + \boldsymbol{\kappa}_I\mathbf{a}_{II} + \mathbf{P}_{IIm2} + z\mathbf{P}_{Ie}\mathbf{c}_I + \mathbf{P}_{IIe}\mathbf{c}_I + \mathbf{P}_{Ie}\mathbf{c}_{II}. \tag{44}$$

In this expression, the symbols that appeared in Eq. (32) have the same values as they did in Eq. (32), except the generalized coefficients. The *new* cross-sectional stiffness influence coefficients κ_{IIij} ($\{i,j\} \subset \{3,\ldots,7\}$), the resultants of the responses to the mechanical loads, and the *new* resultants corresponding to electrical loads can be determined in a similar fashion employed in the uniform-state problem. Here, we only list a few expressions for brevity

$$\kappa_{II3i} = \int_\Omega \mathbf{C}^*[\mathcal{L}_{xy}(\mathbf{\Psi}_{2i}) + \mathcal{L}_z(z\mathbf{\Psi}_{1i})]_{(3)}\,\mathrm{d}x\,\mathrm{d}y, \quad i \in \{3,\ldots,7\}, \tag{45}$$

$$\mathbf{P}_{IIm1}(2) = \int_\Omega \mathbf{C}^*[\mathcal{L}_{xy}(\mathbf{U}_{2m1})]_{(3)}\,y\,\mathrm{d}x\,\mathrm{d}y \tag{46}$$

$$\mathbf{P}_{IIm2}(3) = \int_\Omega \mathbf{C}^*[\mathcal{L}_{xy}(\mathbf{U}_{2m2}) + \mathcal{L}_z(z\mathbf{U}_{2m1})]_{(3)}\,x\,\mathrm{d}x\,\mathrm{d}y \tag{47}$$

$$\mathbf{P}_{IIe}(3,i) = \int_\Omega \mathbf{C}^*[\mathcal{L}_{xy}(\mathbf{\Psi}_{2ei}) + \mathcal{L}_z(z\mathbf{\Psi}_{1ei})]_{(3)}\,x\,\mathrm{d}x\,\mathrm{d}y. \tag{48}$$

In this linear-state problem, the global equilibrium must be evaluated in three stages: First, the rate of change of resultants P_z, M_x, M_y, M_z, and D in Eq. (44) should be equated to the resultant of externally applied axial shear $\hat{P}_z$ per unit length, to applied end forces $\hat{F}_y$ and $\hat{F}_x$, and to the resultants of applied torsional shear $\hat{M}_z$ and the electric displacement per unit length, respectively. To wit,

$$\frac{\partial P_z(z)}{\partial z} = \hat{P}_z, \quad \frac{\partial M_x(z)}{\partial z} = \hat{F}_y, \quad \frac{\partial M_y(z)}{\partial z} = \hat{F}_x, \quad \frac{\partial M_z(z)}{\partial z} = \hat{M}_z, \quad \frac{\partial D(z)}{\partial z} = \hat{D}. \tag{49}$$

Second, setting $z = 0$ yields the resultants at the tip-end, and they should be equal to the applied tip-end loads (since such loads were already considered in the uniform-state problem, they can be set to zero here). Finally, electric loading conditions must be considered; and as before, we illustrate this procedure, in the absence and the presence of electric inputs, respectively, in the following two subsections.

6.2. No electric inputs

Without electric loads, only the first two stages of global equilibrium are needed to determine the solution. To wit,

$$\boldsymbol{\kappa}_I \mathbf{a}_I = \hat{\mathbf{P}}_{II} - \mathbf{P}_{IIm1} \tag{50}$$

with $\hat{\mathbf{P}}_{II} = [\hat{P}_z, \hat{F}_y, \hat{F}_x, \hat{M}_z, 0]^{\mathrm{T}}$,

$$\boldsymbol{\kappa}_{II} \mathbf{a}_I + \boldsymbol{\kappa}_I \mathbf{a}_{II} = -\mathbf{P}_{IIm2}. \tag{51}$$

6.3. With electric inputs

Suppose that linear voltages with gradients $\overline{\Delta\phi_k}$ have been applied along the cylinder. These conditions can be expressed via Eq. (41) as follows

$$\overline{\Delta\phi_k} = \sum_{i=3}^{6} a_{1i}\psi_{1i}(\mathbf{x}_k) + \psi_{2m1}(\mathbf{x}_k) + \sum_{i=1}^{K} c_{1i}\psi_{1ei}(\mathbf{x}_k), \quad k \in \{1,\ldots,K\}. \tag{52}$$

Note that, the terms associated with a_{17} and a_{27} in Eq. (41) will vanish for the present problem. Thus, by combining Eq. (52) with Eq. (50), we get $K+4$ equations for determining the first set of $K+4$ coefficients – a_{1i} ($i \in \{3,4,5,6\}$) and c_{1i} ($i \in \{1,\ldots,K\}$) – denoted by $\mathbf{b}_1$ here, as in

$$\mathbf{K}_I \mathbf{b}_1 = \mathbf{f}_1 \tag{53}$$

where $\mathbf{K}_I$ is identical to the matrix defined in the left-hand side of Eq. (38). The new load vector $\mathbf{f}_1$ is given by

$$\begin{aligned}\mathbf{f}_1 = &\left[\hat{\mathbf{P}}_{II}(1),\ldots,\hat{\mathbf{P}}_{II}(4),\ \overline{\Delta\phi_1},\ldots,\overline{\Delta\phi_K}\right]^{\mathrm{T}} \\ &- [\mathbf{P}_{IIm1}(1),\ldots,\mathbf{P}_{IIm1}(4),\ \psi_{2m1}(\mathbf{x}_1),\ldots,\psi_{2m1}(\mathbf{x}_K)]^{\mathrm{T}}.\end{aligned} \tag{54}$$

After determining $\mathbf{b}_1$, Eq. (51) along with potential conditions evaluated at $z=0$ via Eq. (41) provides the means for determining the second set of coefficients, a_{2i} ($i \in \{3,\ldots,6\}$) and c_{2i} ($i \in \{1,\ldots,K\}$), denoted by $\mathbf{b}_2$ here, as in

$$\mathbf{K}_{II}\mathbf{b}_1 + \mathbf{K}_I \mathbf{b}_2 = \mathbf{f}_2 \tag{55}$$

where

$$\mathbf{K}_{II} = \begin{bmatrix} \boldsymbol{\kappa}_{II}(3:6,3:6) & \mathbf{P}_{IIe}(1:4,1:K) \\ \boldsymbol{\Psi}_{II}(3:6,1:K)^{\mathrm{T}} & \boldsymbol{\Psi}_{IIe}(1:K,1:K) \end{bmatrix}; \quad \mathbf{f}_2 = -[\mathbf{P}_{IIm2}(1:4), \boldsymbol{\psi}_{IIm2}(1:K)]^{\mathrm{T}} \tag{56}$$

with $\boldsymbol{\Psi}_{II}(i,k) = \psi_{2i}(\mathbf{x}_k)$ ($i \in \{3,\ldots,6\}$), $\boldsymbol{\psi}_{IIm2}(k) = \psi_{2m2}(\mathbf{x}_k)$, and $\boldsymbol{\Psi}_{IIe}(i,k) = \psi_{2ei}(\mathbf{x}_k)$ ($i \in \{1,\ldots,K\}$) are the electric potential values at point $\mathbf{x}_k$ extracted from the corresponding warpage $\boldsymbol{\Psi}_{2i}$ ($i \in \{3,\ldots,6\}$), particular solution $\mathbf{U}_{2m2}$, and electric response $\boldsymbol{\Psi}_{2ei}$ ($i \in \{1,\ldots,K\}$) vectors, respectively.

Remark 1. The solution procedures for higher-order (i.e., $k \geqslant 2$) problems have identical steps with those for uniform- and linear-state problems. First, the *functional form* of the solution field $\mathbf{V}_k$ is obtained by integrating that for $\mathbf{V}_{k-1}$ (see, for example Eq. (41)). Second, the warpage functions of $\mathbf{V}_k$ are obtained by solving a sequence of linear problems that involves the warpage functions of $\mathbf{V}_{k-1}$ (see, for example, Eq. (42)). Finally, the unknown coefficients of $\mathbf{V}_k$ are obtained via global equilibrium equations, and the prescribed electromechanical loads appropriate for the k-th order problem (see, for example, Eq. (55)).

Remark 2. It also appears possible to obtain *approximate* solutions for loads with non-polynomial axial variations through a least-squares based superposition of polynomial loads. However, the polynomial states may have to be made orthogonal first (for example, via the Gram–Schmidt procedure) in order to obtain efficient and accurate approximations.

7. Verification problems and an application example

7.1. Verification problems for the uniform- and linear-state problems

In order to verify the semi-analytic meshfree method and its implementation, we compare its results with those obtained via three-dimensional finite element analyses (using ANSYS, 1998) for a set of basic problems. We consider a piezoelectric 'bimorph' with a length-to-thickness ratio $L/t = 10$, and width-to-thickness ratio $w/t = 2$, as shown in Fig. 2a. Both layers of the bimorph are made of PZT4 (Lead–Zirconium–Titanate) and its material properties may be found in Ikeda (1996). Two typical layer arrangements are shown in Fig. 2b – which is a *serial (anti-parallel) bimorph* that has positive and negative y-direction polarizations for its top and bottom layers, respectively – and in Fig. 2c – which is a *parallel bimorph* that has a grounded electrode at the layer interface and both of its layers are polarized in the positive y-direction. Fig. 2d displays the cross-sectional configuration and its meshfree discretization. In the semi-analytical method, 99 meshfree particles were used, while in ANSYS the domain was discretized with 4000 ($10 \times 10 \times 40$) finite elements. For problems presented here, we adopt the normalization procedure outlined in Bai et al. (2004) so that the material properties, applied loads, and the solution fields are dimensionless.

For the uniform-state problem, we considered the complete set of mechanical loads – i.e., axial end force ($F_z = 1.0$), end moments ($M_x = 1.0, M_y = 1.0$), end torque ($T_z = 1.0$), and uniform pressure ($P = 1.0$). Additionally, we analyzed the serial bimorph's response under a uniform voltage ($V = 1.0$) applied on its top surface with its bottom surface grounded, and the parallel bimorph's response under uniform voltages ($V = 1.0$) applied on its top and bottom surfaces with its interface grounded. The solutions obtained at $z = 5.0$ are presented in Figs. 3 and 4. In each of these figures, columns 1 and 2 comprise semi-analytic and ANSYS solutions, respectively, where the deformed shapes of the cross-section, and the variations of electric potential (indicated by color) are presented; column 3 contains variations of normalized displacements and potential within the cross-section – sampled along the diagonal (dashed) line shown in Fig. 2b. As these results indicate there is excellent agreement between semi-analytic and three-dimensional finite element solutions for all loading cases of the uniform-state problem.

For the linear-state problem, we analyzed the serial bimorph (parallel bimorph results are omitted for brevity) and considered the complete set of mechanical loads – i.e., end forces ($F_x = 1.0, F_y = 1.0$), axial uniform shear along the lateral surfaces ($\overline{S_z} = 1.0$), and linear pressure ($\overline{\Delta P} = 1.0$). Additionally, we considered a linearly varying voltage ($\overline{\Delta V} = 1.0$) applied along the bimorph's top and bottom surfaces. The solutions obtained at $z = 5.0$ are presented in Fig. 5; and again, the agreement between semi-analytic and finite element solutions is excellent.

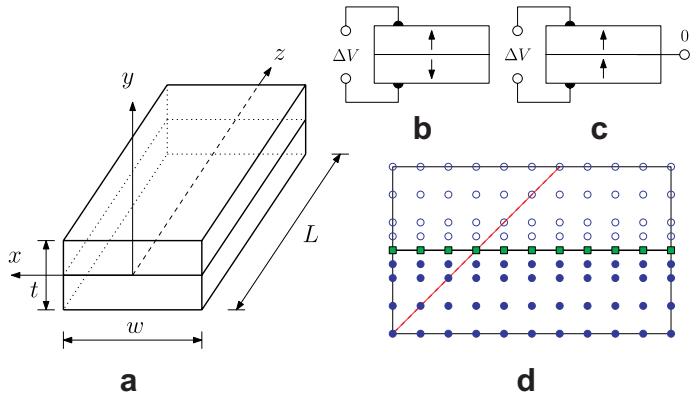

Fig. 2. Two-layer bimorph cantilever. (a) Geometry, (b) series arrangement, (c) parallel arrangement, and (d) cross-sectional discretization.

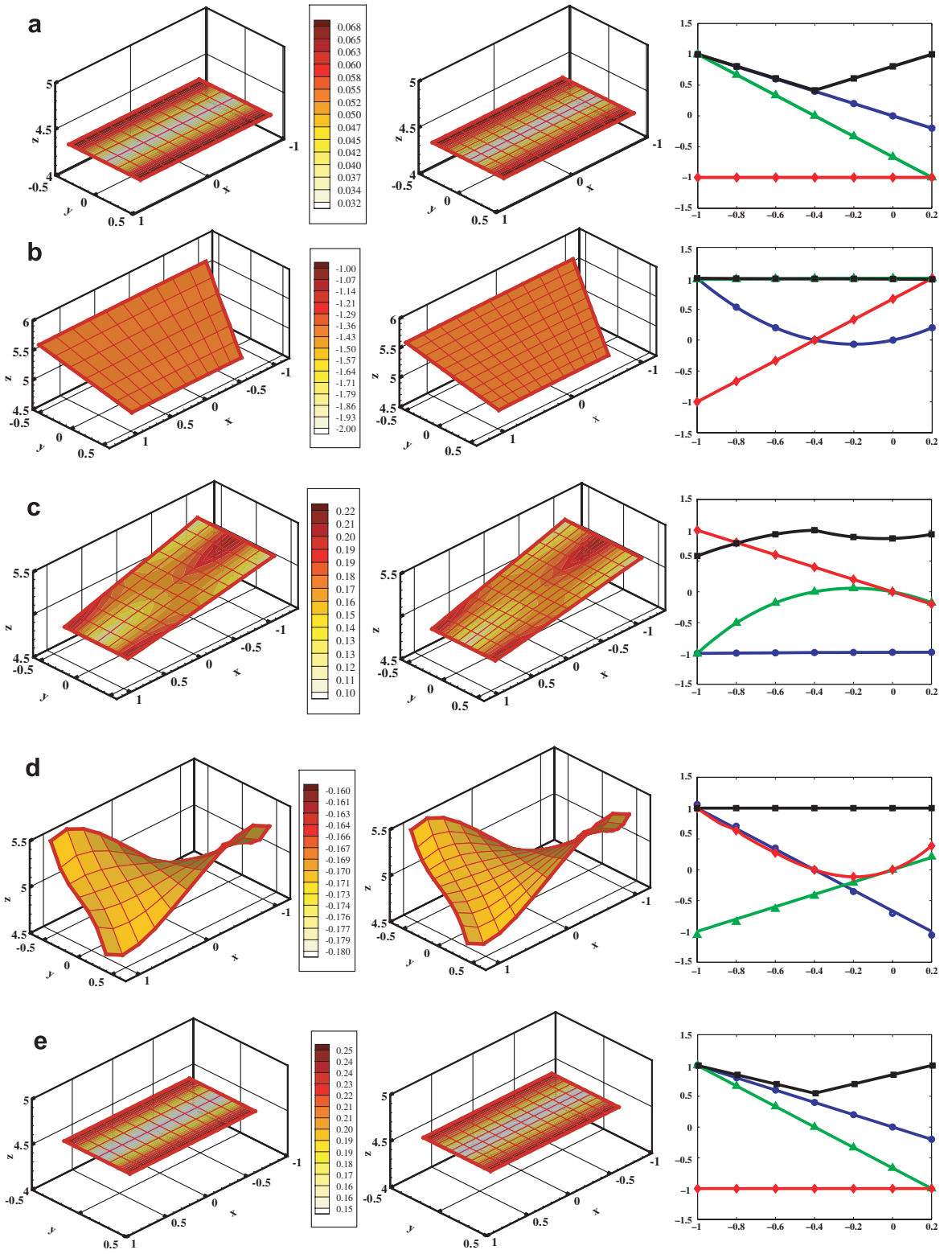

Fig. 3. Verification results (semi-analytic in column 1; ANSYS in column 2) for uniform-state problems due to prescribed axial end force F_z (a), end moments M_x (b), and M_y (c), end torque T_z (d), and uniform pressure (e). In column 3, the symbols (◯, u; △, v; ◇, w; □, ϕ) and the lines denote semi-analytic and ANSYS solutions, respectively.

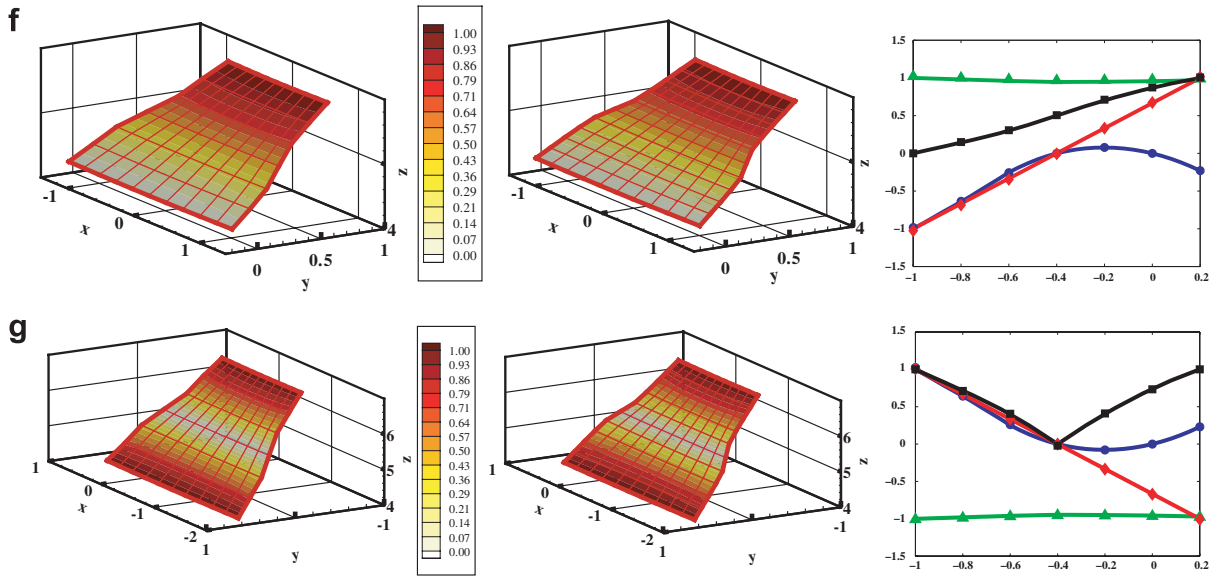

Fig. 4. Verification results (semi-analytic in column 1; ANSYS in column 2) for uniform-state problems due to prescribed uniform voltage for the serial (f) and parallel (g) bimorphs. In column 3, the symbols (◯, u; △, v; ◇, w; □, ϕ) and the lines denote semi-analytic and ANSYS solutions, respectively.

7.2. Verification problem: flexure of a homogeneous beam with rectangular cross-section

Exact solutions for Saint-Venant problems involving non-circular cross-sections or high-orders of anisotropy are quite rare. One such solution that exists is for the flexure of a cylinder which is homogeneous but with a rectangular cross-section. Before we present an application example in the subsequent section, we would like to investigate the said problem.

Consider a homogeneous rectangular beam, with its axes labeled as in Fig. 2a. The beam is with length $L = 10$, width $w = 2$, and thickness $t = 1$. It is made of an elastic material with $E = 1$ and $v = 0.3$. It is fixed at $z = 0$, and subjected to a resultant end force at $z = 10$ with magnitude $F_y = -1$. The three-dimensional stress field of this problem is given by Sokolnikoff (1956), as follows:

$$\begin{aligned}
&\sigma_{11} = \sigma_{22} = \sigma_{12} = 0;\\
&\sigma_{33} = -\tfrac{p}{I_x}(L-z)y;\\
&\sigma_{23} = -\tfrac{p}{2(1+v)I_x}\left[\tfrac{1}{2}v(y^2-x^2) + \tfrac{\partial \Phi}{\partial y} + x^2 - z^2 + 2Lz\right];\\
&\sigma_{13} = -\tfrac{p}{2(1+v)I_x}\left[(2+v)xy + \tfrac{\partial \Phi}{\partial x}\right]
\end{aligned} \tag{57}$$

where the area moment of inertia is $I_x = wt^3/12$, and the flexure function $\Phi(x,y)$ has the form

$$\Phi(x,y) = \left[-\frac{1}{4}(1+v)t^2 + \frac{1}{12}vw^2\right]y + \frac{vw^3}{2\pi^3}\sum_{n=1}^{\infty}\frac{(-1)^n}{n^3}\frac{\sinh\frac{2n\pi y}{w}}{\cosh\frac{n\pi t}{w}}\cos\frac{2n\pi x}{w} + \frac{1}{6}(2+v)(y^3 - 3x^2y). \tag{58}$$

Fig. 6 displays the stresses within the cross-section at midspan (i.e., $z = 5$) – sampled along the diagonal (dashed) line shown in Fig. 2b. These results are obtained through the present semi-analytic method and Eq. (57) and good agreement between the two is evident.

7.3. An application example

In order to demonstrate the utility of the proposed semi-analytical method, we analyze a piezoelectric sensor/actuator device. As shown in Fig. 7, the simple device has the dimensions $L = 5$ cm and $w = 1$ cm, and

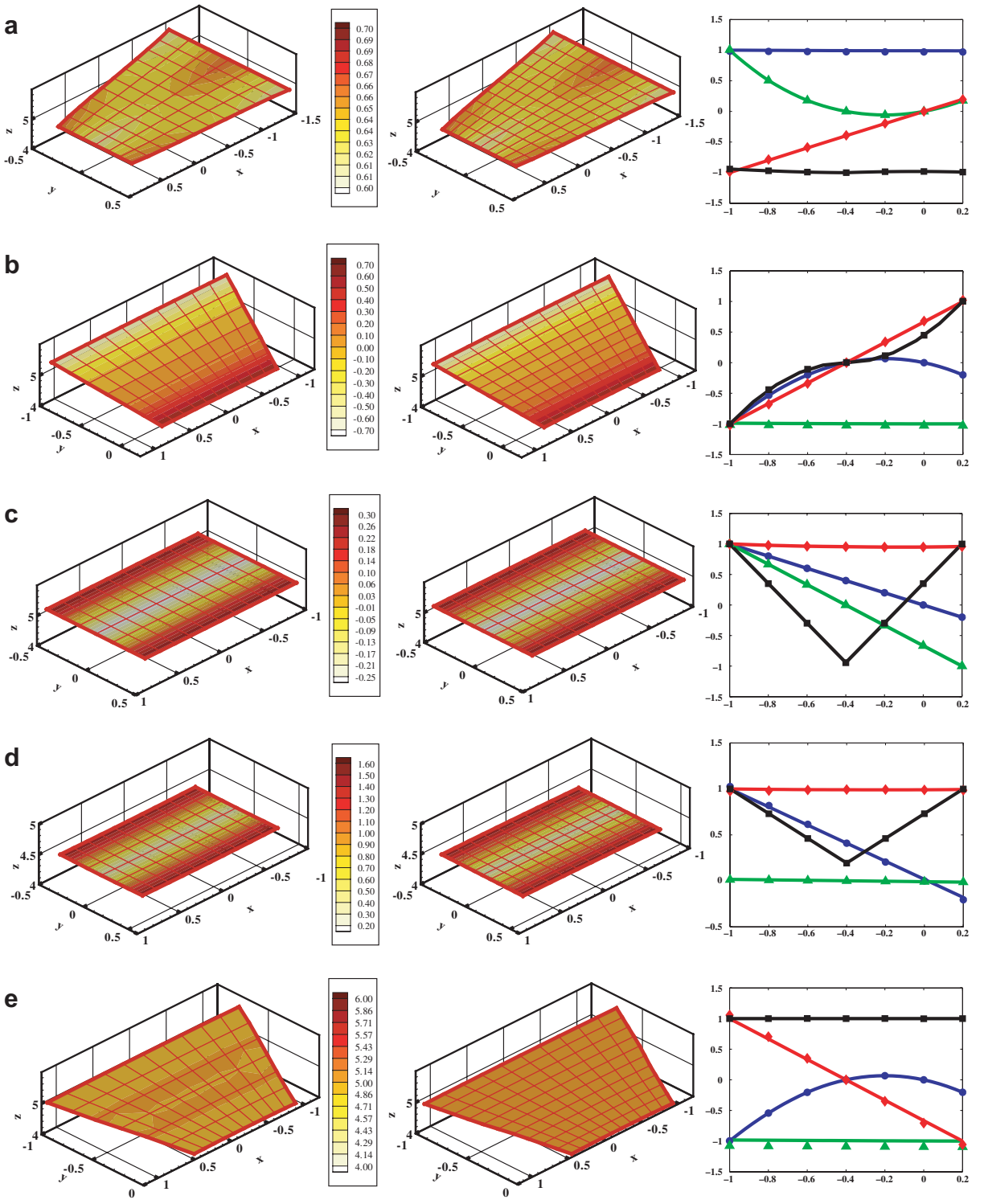

Fig. 5. Verification results (semi-analytic in column 1; ANSYS in column 2) for linear-state problems due to prescribed end force F_x (a), end force F_y (b), linear pressure (c), axial shear (d) prescribed on the surface, and linear voltage (e) for the serial bimorph. In column 3, the symbols (◯, u; △, v; ◇, w; □, ϕ) and the lines denote semi-analytic and ANSYS solutions, respectively.

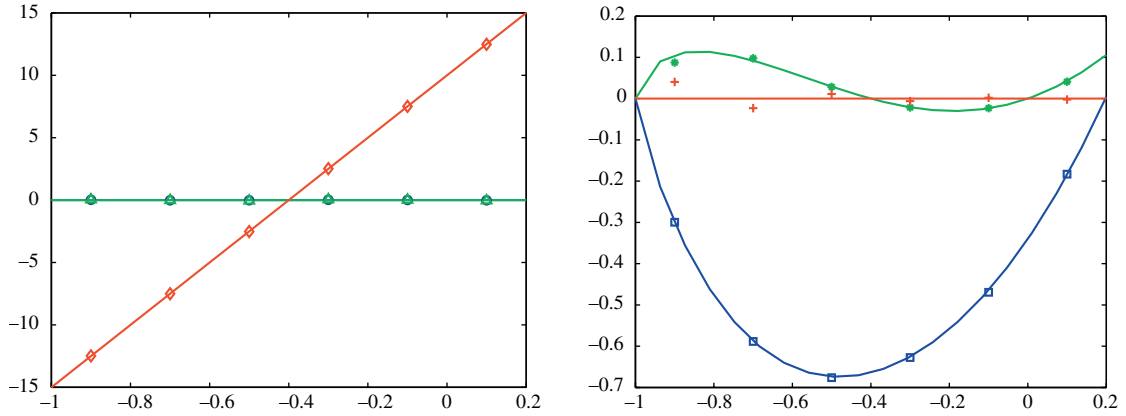

Fig. 6. Verification results: lines and symbols ($\bigcirc, T_{xx}$; $\triangle, T_{yy}$; $\diamondsuit, T_{zz}$; $\square, T_{yz}$; $*, T_{xz}$; $+, T_{xy}$) denote analytical and semi-analytic solutions, respectively.

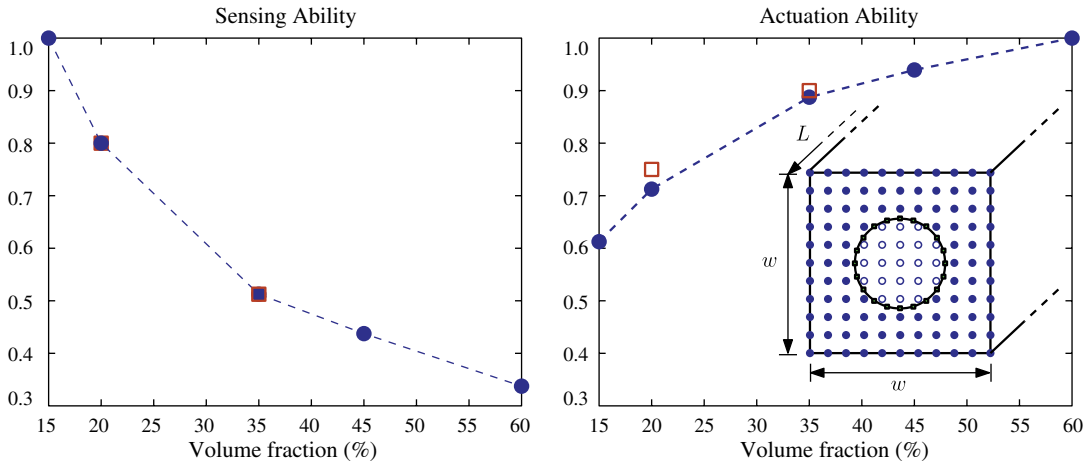

Fig. 7. Piezoelectric device with a circular PZT5 fiber: variations of sensing and actuation abilities with respect to fiber volume fraction. Lines (with circles) and square symbols denote semi-analytic and ANSYS solutions, respectively.

comprises a cylindrical piezoelectric fiber embedded in a soft elastic medium. The axially polarized piezoelectric fiber is made of PZT5 (for material properties, see Ikeda, 1996), and the elastic medium has a Young's modulus of $E = 7.0 \times 10^9$ Pa, and a Poisson's ratio of $\nu = 0.35$. When an axial force is applied at the end, a potential gradient will be generated in which case the resulting the voltage difference between the two ends can be measured. On the other hand, an axial displacement/force will be generated when a voltage is applied at one end and while the other end is grounded. Thus, the device is both a sensor and an actuator.

Here, we simply define device 'sensing ability' as the generated voltage difference when a unit force is applied, and 'actuation ability' as the generated displacement when unit voltage is prescribed at one end. Fig. 7 displays the sensing and actuation abilities of the device for different piezoelectric fiber volume fractions, $V_p/V = [0.15, 0.20, 0.35, 0.45, 0.60]$ (in all cases, the fiber is circular and located at the center). Several cases are also analyzed via ANSYS in order to verify the semi-analytic solutions (these results are shown in figure as square symbols). We note that, in semi-analytic meshfree calculations, discretization of successive problem geometries were achieved by simply relocating the bi-material interface curve. In contrast, all three-dimensional finite element geometries had to be generated from scratch. Moreover, the proposed approach 7–8 times faster than ANSYS for this particular problem, while noting that our computer code used in these calculations was not optimized.

From these results, we can conclude that the 'optimized' fiber volume fraction is near 30%, which brings about relatively large simultaneous sensing and actuation abilities. A more difficult, and compelling, optimization problem would have been to allow topology changes in both the piezo-fiber and the cover material. While it is possible to tackle such a problem with the proposed semi-analytic meshfree method, it is beyond the scope of the present study; and we defer the treatment of such problems to a subsequent publication.

8. Conclusions

A semi-analytical meshfree method is developed for analyzing the behavior of prismatic piezoelectric cylinder with general cross-sectional geometry under polynomially varying lateral surface, and resultant-based end loads. The method is based on a meshfree discretization of the cylinder's cross-section, and the analytical determination of the electromechanical fields along the axial direction. The provided verification problems affirm the validity of this approach. The utility of the method is demonstrated in a problem whereby the optimum fiber volume fraction that maximizes the simultaneously sensing and actuation abilities of a device is obtained. The proposed semi-analytical method provides significant computational savings in comparison to fully discrete methods, and is more general than structural theory-based methods. It is also ideal for formal optimum problems of prismatic smart structures, as the sensitivity computations of externally defined design objective functions, and successive topology changes can be performed in a straightforward fashion.

Acknowledgments

This study is supported by funding from Faculty Grants Program of UCLA Academic Senate Council on Research, and in part, by NSF award CMS-0547670. The contents of this article do not necessarily reflect the opinions of the sponsors. The authors thank Professor Stanley B. Dong for sharing his invaluable insights into the subject matter. The computer codes used in generating the results with the semi-analytic method presented in this paper are available on request from the authors.

References

Allik, H., Hughes, T.J.R., 1970. Finite element method for piezoelectric vibration. Int. J. Numer. Meth. Eng. 2, 151–157.

Almansi, E., 1901. Sopra la deformazione dei cilindri solecitati lateralmente. Atti Reale Acad. naz. Lincei Rend. Cl. Sci. Fis., Mat. e Natur. Ser. 5 10, I: 333–338, II: 400–408.

ANSYS, 1998. Coupled-Field Analysis Guide, third ed. ANSYS Release 5.5.

Bai, H., Taciroglu, E., Dong, S.B., Shah, A.H., 2004. Elastodynamic Green's functions for a laminated piezoelectric cylinder. Int. J. Solids Struct. 41, 6335–6350.

Belytschko, T., Lu, Y.Y., Gu, L., 1994. Element-free Galerkin methods. Int. J. Numer. Meth. Eng. 37, 229–256.

Benjeddou, A., 2000. Advances in piezoelectric finite element modeling of adaptive structural elements: a survey. Comput. Struct. 76, 347–363.

Bisegna, P., 1998. The Saint-Venant problem for monoclinic piezoelectric cylinders. Z. Angew. Math. Mech. 3, 147–165.

Bobaru, F., Mukherjee, S., 2001. Shape sensitivity analysis and shape optimization in planar elasticity using the element-free Galerkin method. Comput. Meth. Appl. Mech. Eng. 190, 4319–4337.

Borri, M., Merlini, T., 1986. A large displacement formulation for anisotropic beam analysis. Meccanica 21, 30–37.

Cesnik, C.E.S., Shin, S., 2001. On the modeling of integrally actuated helicopter blades. Int. J. Solids Struct. 38, 1765–1789.

Daví, F., 1996. Saint-Venant's problem for linear piezoelectric bodies. J. Elasticity 43, 227–245.

Dong, S.B., Kosmatka, J.B., Lin, H.C., 2001. On Saint-Venant's problem for an inhomogeneous, anisotropic cylinder – part I: methodology for Saint-Venant solutions. ASME J. Appl. Mech. 68, 376–381.

Giavotto, V., Borri, M., Mantegazza, P., Ghiringhelli, G., Carmaschi, V., Maffioli, G.C., Mussi, F., 1983. Anisotropic beam theory and applications. Comput. Struct. 16, 403–413.

Ghiringhelli, G.L., Masarati, P., Mantegazza, P., 1997. Characterisation of anisotropic, non-homogeneous beam sections with embedded piezo-electric materials. J. Intell. Mater. Syst. Struct. 8, 842–858.

Huang, C.H., Dong, S.B., 2001. Analysis of laminated circular cylinders of materials with the most general form of cylindrical anisotropy: I. axially symmetric deformations. Int. J. Solids Struct. 38, 6163–6182.

Ieşan, D., 1986. On Saint-Venant's problem. Arch. Ration. Mech. Anal. 91, 363–373.

Ieşan, D., 1987. Saint-Venant's Problem. Lecture Notes in Mathematics. Springer, Heidelberg.

Ikeda, T., 1996. Fundamentals of Piezoelectricity. Oxford University Press, Oxford, UK.

Krongauz, Y., Belytschko, T., 1998. EFG approximation with discontinuous derivatives. Int. J. Numer. Meth. Eng. 41, 1215–1233.

Liu, C.W., Taciroglu, E., 2006. Enriched reproducing kernel particle method for piezoelectric structures with arbitrary interfaces. Int. J. Numer. Meth. Eng. 67 (11), 1565–1586.

Liu, C.W., Taciroglu, E., 2007. Numerical analysis of end-effects in laminated piezoelectric circular cylinders. Comput. Meth. Appl. Mech. Eng. 196 (17–20), 2173–2186.

Liu, W.K., Jun, S., Zhang, Y.F., 1995. Reproducing kernel particle methods. Int. J. Numer. Meth. Fluids 20, 1081–1106.

Michell, J.H., 1901. The theory of uniformly loaded beams. Q. J. Math. 32, 28–42.

Popescu, B., Hodges, D.H., 1999. On asymptotically correct Timoshenko-like anisotropic beam theory. Int. J. Solids Struct. 37 (3), 535–558.

Saravanos, D.A., Heyliger, P.R., 1995. Coupled layerwise analysis of composite beams with embedded piezoelectric sensors and actuators. J. Intell. Mater. Syst. Struct. 6, 350–363.

Saravanos, D.A., Heyliger, P.R., 1999. Mechanics and computational models for laminated piezoelectric beams, plates, and shells. Appl. Mech. Rev. 52, 305–320.

Saint-Venant, A.J.C.B.D., 1855. Memoire sur la torsion des prismes. Memoire des Savants Etrangers, Acad. Sci. Paris 14, 223–560.

Saint-Venant, A.J.C.B.D., 1856. Memoire sur la flexion des prismes. J. Math. Liouville 1, 89–189.

Sokolnikoff, I.S., 1956. Mathematical Theory of Elasticity. McGraw-Hill, New York.

Taciroglu, E., Liu, C.W., Dong, S.B., Chun, C.K., 2004. Analysis of laminated piezoelectric circular cylinders under axisymmetric mechanical and electrical loads with a semi-analytic finite element method. Int. J. Solids Struct. 41, 5185–5208.

Taciroglu, E., Liu, C.W., 2005. Analysis and design of multimodal piezoelectric layered tubular sensors and actuators. Smart Mater. Struct. 14, 605–614.

Tarn, J.Q., 2002. Exact solutions of a piezoelectric circular tube or bar under extension, torsion, pressuring, shearing, uniform electric loading and temperature change. Proc. R. Soc. Lond. A 458, 2349–2367.

Tiersten, H.F., 1969. Linear Piezoelectric Plates. Plenum Press, New York.

Wang, D., Chen, J.S., Sun, L., 2003. Homogenization of magnetostrictive particle-filled elastomers using an interface-enriched reproducing kernel particle method. Finite Elem. Anal. Des. 39, 765–782.

Yu, W., Hodges, D.H., 2004. Elasticity solutions versus asymptotic sectional analysis of homogeneous, isotropic, prismatic beams. J. Appl. Mech. 71, 15–23.

Yu, W., Hodges, D.H., Volovoi, V., Cesnik, C.E.S., 2002. On Timoshenko-like modeling of initially curved and twisted composite beams. Int. J. Solids Struct. 39, 5101–5121.